METHODS 19, 234–252 (1999)
Article ID meth.1999.0854, available online at http://www.idealibrary.com on IDEAL®

Fluorescence Fluctuation Spectroscopy

Yan Chen,*,[1] Joachim D. Müller,* Keith M. Berland,† and Enrico Gratton*

*Laboratory for Fluorescence Dynamics, University of Illinois at Urbana–Champaign, Urbana, Illinois, 61801; and †T. J. Watson Research Center, Yorktown Heights, New York 10598

The analysis of the intensity fluctuation of a fluorescence signal from a relatively small volume and from a few molecules contains information about the distribution of different species present in the solution and about kinetic parameters of the system. The same information is generally averaged out when the fluorescence experiment is performed in a much larger volume, typically a cuvette experiment. The fundamental reason for this difference is that the fluctuations of the fluorescence signal from a few molecules directly reflect the molecular nature of the matter. Only recently, with the advent of confocal microscopy and two-photon excitation, it has become practical to achieve small excitation volumes in which only a few fluorescent molecules are present. We introduce the concept of fluctuation spectroscopy and highlight some of the technical aspects. We discuss different analysis methods used in fluctuation spectroscopy and evaluate their use for studying protein–protein interactions.

Fluorescence fluctuation spectroscopy is an emerging technique with potential applications for the study of protein–protein interactions. The two most important parameters determined by the autocorrelation function of the fluorescence fluctuations are the diffusion coefficient D and the $G(0)$ value, which is related to the average number of molecules within the excitation volume $\bar{N}$. Association of proteins to form oligomers changes the molecular mass, thus slowing down the diffusion. The change in the average number of molecules, however, is a far more sensitive parameter. We show in this contribution how the number of molecules $\bar{N}$ can be used to characterize the equilibrium between a protein dimer and its tetramer. Another useful approach is to separate species by their inherent fluorescence intensity. If each monomer is labeled individually with a fluorescent dye, then dimers display higher fluorescence intensities than monomers. The intensity distribution is captured by the photon counting histogram. Here we introduce the concept of the photon counting histogram analysis, which has been recently developed in our group (1), and point out its strength in separating species on the basis of the difference in their molecular brightness. However, before we discuss these issues let us start with an introduction to fluctuation spectroscopy.

1.1. Fluctuation Spectroscopy

Fluctuation spectroscopy started at the beginning of this century with the invention of the ultramicroscope. This instrument permitted for the first time the detection and study of particles with a diameter less than 0.1 μm (2). Subsequent experiments with the ultramicroscope by Perrin and others beautifully confirmed the theory of Brownian motion and diffusion developed by Einstein and von Smoluchowski (3).

To illustrate the concept of fluctuation spectroscopy we choose data from an experiment by Svedberg and Inouye on gold colloids (4). The diameter of the gold particles was estimated to be only 6 nm. Obviously, this size is too small to allow direct observation of the particles. But the scattering of light induced by such submicron particles can be detected in the ultramicroscope. A small slit in the detection path defines the observation volume. If a particle enters the observation volume, it scatters light into the eyepiece of the microscope and can be detected by the dark-adapted human eye. In that particular experiment the number of particles simultaneously present in the observation volume was counted 39 times per minute, and the recorded data are as follows:

[1] To whom correspondence should be addressed at Laboratory for Fluorescence Dynamics, 184 Loomis Laboratory, 1110 West Green, Urbana, IL 61801. Fax: (217) 244–7187. E-mail: yan@lfd.physics.uiuc.edu.

1046-2023/99 $30.00

1200020013241231021111311251110233133322l
1122422122612214234524114131142310010042112 31
23201111000111–211001320000010011000100023221
002110000201001–33312200023122102401110 2–1222
1122310001103311102101100101030113121210101 2
1111211–10003221012302012121321110110023312 24
2110001203010100221734410101002112211444421 21
1440132123314313011222123310121111222412231 11
3322132110000410432012120011322231200–253212
0332331111002100220130113211312001013143221 12
2112232344222303214215322002021421232320431 12
3120033142234521341104123222202 21

The dashes indicated where the observer took a break for his eyes.

The numbers of particles are displayed in Fig. 1A as a function of time. The raw data of the fluctuation experiment are of rather limited practical use. It is almost impossible to extract information about the physics of fluctuations by staring at the data stream.

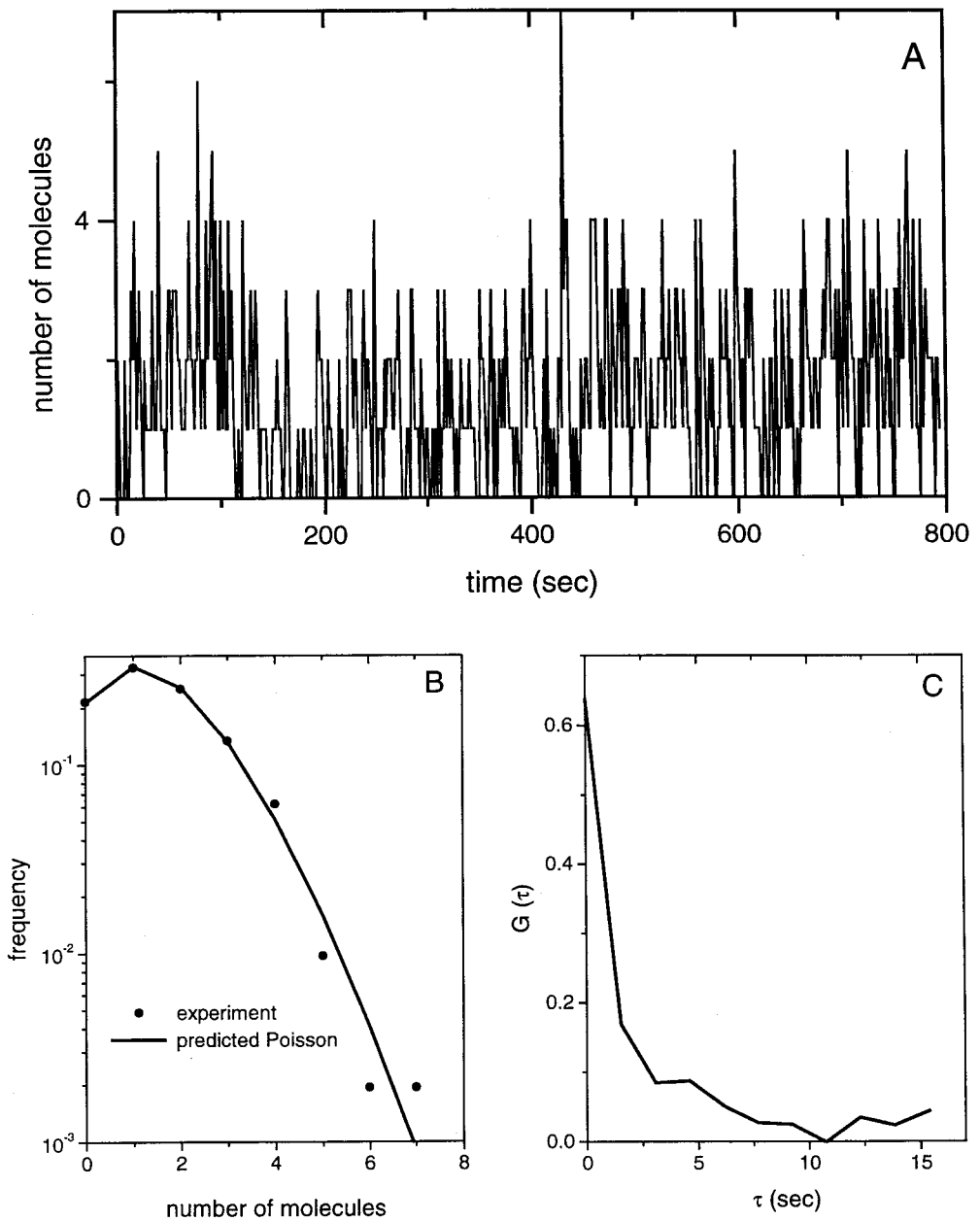

FIG. 1. Experimental data from Svedberg and Inouye on gold colloids. (A) Time sequence of the number of particles observed. (B) Histogram of the detected number of particles. The Poisson distribution is calculated for an average of 1.55 particles. (C) Autocorrelation function, $G(\tau)$, of the particle fluctuations.

Therefore, it is necessary to perform a statistical analysis of the data to condense and emphasize particular aspects of the experiment. In the following we discuss different representations of the same data set: the histogram, the moments, and the autocorrelation function, $G(\tau)$, of the data.

The normalized histogram describes the probability of observing N particles in the observation volume and is shown in Fig. 1B. For a small excitation volume, which can freely exchange particles with its surrounding bath, a Poissonian distribution of particles is expected:

$$p(N) = \frac{\overline{N}^N \cdot \exp(-\overline{N})}{N!}. \qquad [1]$$

The original formulation of this law is due to work by Einstein and von Smoluchowski (3).

A fit of the histogram data by a Poisson distribution shows good agreement between theory and experimental data and yields an average of 1.55 molecules in the observation volume. Actually, the very same data presented above were used by von Smoluchowski to examine the Poissonian character of number fluctuations from a theoretical point of view (5). The statistical independence of the particles is a requirement for Poissonian number fluctuations and only realized in ideal solutions.

The autocorrelation function, $G(\tau)$, characterizes the time-dependent decay of fluctuations to their equilibrium value. More specifically, it calculates the similarity between a signal and a copy of the same signal, but shifted by a time lag τ. Here we are concerned about the number of particles $N(t)$ and its autocorrelation, given by

$$G(\tau) = \frac{\langle N(t) \cdot N(t+\tau)\rangle - \langle N(t)\rangle^2}{\langle N(t)\rangle^2} = \frac{\langle \delta N(t) \cdot \delta N(t+\tau)\rangle}{\langle N(t)\rangle^2}, \qquad [2]$$

where $\delta N(t) = N(t) - \langle N\rangle$ expresses the fluctuation in the particle number at time t. At the time the experiment was performed all calculations were carried out by hand, and the determination of the autocorrelation function was a very demanding task. Today, the autocorrelation function $G(\tau)$ is simply calculated by a computer and is shown for the experimental data in Fig. 1C.

Let us choose the $1/e$ point of the autocorrelation function as the characteristic diffusion time of the particles through the observation volume. From the curve in Fig. 1C we arrive at a characteristic diffusion time of 1.5 s, which characterizes the average residence time of the particle inside the detection volume. The particle number fluctuations are due to Brownian motion of the particles in the solution. The Stokes–Einstein relationship predicts a diffusion coefficient of 60 $\mu m^2/s$ for the estimated particle diameter of 6 nm in aqueous solution.

The time zero value of the autocorrelation function $G(0)$ represents the normalized variance $\langle \Delta N^2\rangle/\bar{N}^2$. The number fluctuations obey Poissonian statistics. As a consequence, the $G(0)$ value is the inverse of the number of molecules in the detection volume:

$$G(0) = \frac{1}{\overline{N}}. \qquad [3]$$

The recovered $G(0)$ of 0.64 for the experimental data indicates that there are 1.56 particles in the observation volume, which is almost identical to the average particle number of 1.55. Note the absence of shot noise in this experiment.

The above data are taken from one of the earliest fluctuation experiments. The technique matured since then and has been applied to many different subjects, such as Johnson noise (6, 7), the Barkhausen effect (8), $1/f$ noise (9), mutation in bacteria (10), and spin glasses (11), to name only a few.

1.2. Fluorescence Fluctuation Spectroscopy

Modern instrumentation has changed fluctuation spectroscopy significantly. Electronic detectors have replaced the human eye, lasers are used instead of sunlight, and digital computers eradicated paper and pencil. However, the conceptual basis of fluctuation spectroscopy has not changed much. Moments, probability distributions, and correlation functions are still most commonly used to describe stochastic processes (12). Instead of counting particles directly, modern detectors measure intensities or photon counts, thus introducing an additional layer of abstraction. Consequently, the theory has to be adapted to reflect the detection process.

Here, we will not measure scattering as in the historic experiment, but study fluorescence. The scattering cross section decreases strongly with the size of the particle, and materials other than gold or silver scatter light rather weakly, thus limiting this technique to a few materials or large structures. The possibility of detecting single molecules was already addressed in the original article by Siedentopf and Zsigmondy on the ultramicroscope. They concluded that scattering techniques are not suitable, but that fluorescence could be a promising candidate.

Indeed, 70 years later, Magde and co-workers (13, 14) introduced fluorescence correlation spectroscopy (FCS) and applied the technique to investigate the diffusion and binding of ethidium bromide to double-

stranded DNA. The inherent sensitivity and specificity of fluorescence spectroscopy suit this technique for fluctuation studies. The necessity to keep the average number of particles in the observation volume small and to reject background signal at the same time requires small volumes. The implementation of confocal (15–17) and two photon microscopy (18) with their tiny observation volumes ($V \approx 1\ \mu m^3$) greatly increased the sensitivity of FCS and pushed the detection limit to the single molecule level (19, 20).

While the temporal behavior of fluctuations is best described by the autocorrelation function, the amplitude of the fluctuations is characterized by its probability distribution. However, the experimentally collected photon stream contains shot noise as a consequence of the detection process. To recover the information embedded in the photon shot noise, a theory of the photon count distribution was developed (1).

1.2.1. Autocorrelation Analysis

The time-dependent decay of the fluorescence intensity fluctuations is characterized by the autocorrelation function $G(\tau)$, which is directly obtainable from FCS experiments. Theoretical models for a number of physical processes, such as diffusion and chemical reactions, exist (14, 21, 22). FCS has been applied to study translational and rotational diffusion (23, 24), flow (25), chemical reactions (26), triplet state kinetics (27), and hybridization reactions (28, 29). It has been applied to study processes in bulk solution, on surfaces and in cells (24, 30, 31). In the case of pure translational diffusion of a single species, two parameters can be recovered from the autocorrelation function: the average number of molecules $\bar{N}$ in the observation volume, which is given by $1/G(0)$, and the diffusion coefficient D of the particles (32, 33).

1.2.2. PCH Analysis

While the temporal behavior of fluctuations is best described by the autocorrelation function, the amplitude of the fluctuations is characterized by its probability distribution. Here we are specifically interested in the probability distribution to detect k photons per sampling time during fluorescence fluctuation experiments. This probability is experimentally determined by the histogram of the detected photons, which we call the photon counting histogram (PCH).

The probability of detecting k photoelectrons $p(k)$ in fluorescence fluctuation experiments has so far received relatively little attention (34, 35). We have developed (1) a theoretical expression for the photon counting histogram based on the theory of photon detection (36). We show that two parameters uniquely characterize the distribution of photon counts for a single chemical species. The first parameter is the average number of molecules in the observation volume, $\bar{N}$, the second parameter is given by the molecular brightness ϵ, defined as the average number of detected photons per sampling time per molecule.

We have generalized the theory of the photon counting histogram to a mixture of species and demonstrated it experimentally for the case of two species. The autocorrelation function offers a way to separate chemically different species, if their diffusion coefficients differ substantially. PCH analysis offers another way to distinguish between different species, which is based on the brightness difference of the different molecular species, but not on the temporal behavior of the fluctuations. PCH analysis can thus provide information not accessible through the autocorrelation function. In many cases of biological interest, the contrast given by the difference in brightness between two species is larger than the contrast given by the difference in their diffusion coefficients.

1.2.3. Moment Analysis

Moments provide a model-independent way to characterize probability distributions. The first moment marks the average of the distribution, while the second central moment, the variance, describes the width of the distribution. These are the two most important moments from a practical standpoint. There are also higher order moments, like the third moment, which represents the skewness of a distribution (37).

It is, in principle, possible to calculate the values of $G(0)$ directly from the first and second moments of the fluorescence intensity distributions. Experimentally, we obtain photon counts instead of intensities, and the shot noise contribution to the photon counts must be taken into consideration. By using the well-known relationship between the factorial moments of the photon counts and the ordinary moments of the light intensity, the shot noise contribution can be accounted for by a simple algebraic operation (35, 38). The main advantages of this direct calculation of $G(0)$ from the first and second moments are its computational simplicity and model independence. It is easy to implement moment analysis into the data acquisition program, which proves very helpful in judging the quality of the data on the fly.

1.3. Protein–Protein and Protein–Ligand Interactions

Molecular interactions are at the heart of all biological systems, and are essential for processing and storing information, assembling structures, and regulating physiological processes. Fluorescence techniques have been widely used to investigate the intermolecular interaction of proteins. Titration experiments, where the concentration of one component is systematically varied, provide information about cooperativity and the binding energy of the reaction. The contribution of each component to the measured signal depends on the tech-

nique used. Fluorescence intensities are simply added together, while each anisotropy has to be scaled by the fractional intensity of the species (39, 40). The autocorrelation function $G(\tau)$ of a binary mixture is, on the other hand, given by the superposition of the individual autocorrelation functions weighted by their fractional intensity squared (41). The PCH of a mixture is the convolution of all individual counting histograms, as we will show later in this contribution.

FCS has been used to investigate the acetylcholine receptor binding to α-bungarotoxin based on the difference in the diffusion coefficient between the bound and free ligand (42). However, the diffusion coefficient scales approximately with the cubic root of the molecular weight. Thus, FCS cannot resolve reactions involving only small changes in the molecular weight. Consequently it is impractical to resolve monomer–dimer mixtures based on the autocorrelation function alone.

We have explored an alternative approach to analyze titration data based on the $G(0)$ value, a method that has received very little attention so far (43). We applied PCH or moment analysis to recover $G(0)$ from the fluctuation data of the mixture of antibodies and their antigen. In addition, we characterized the molecular brightness ϵ and the average number of molecules $\bar{N}$ of the ligand alone. With this information a simultaneous fit of the $G(0)$ and intensity titration curve was performed, which allowed us to recover the dissociation constant K_D, and the number of binding sites and to examine the heterogeneity of the liganded protein (44). Later in this contribution we apply the concept of $G(0)$ analysis to characterize the dimer–tetramer equilibrium of glycogen phosphorylase A.

2. EXPERIMENTAL CONSIDERATIONS

2.1. Two-Photon Excitation

Macroscopic systems typically do not allow the observation of fluctuations, because of the enormous number of independent contributions that make up the observable. In the microscopic world, however, fluctuations are abundant. Therefore, to perform FCS experiments, extremely small volumes containing only a few molecules are required.

When FCS was introduced in the early 1970s (13, 14), the instabilities of the laser systems used for excitation of fluorophores made it difficult to perform measurements. It was also not possible to achieve very small excitation volumes with the instrumentation available at that time. The early FCS experiments were limited largely to two-dimensional (2D) systems. FCS became more widespread in the early 1990s with the commercial availability of confocal microscopes and Ti:sapphire laser systems (15, 17, 18). Two-photon excitation and confocal microscopy provide both high axial resolution and extremely small detection volumes. For these systems, typical detection volumes are on the order of 0.1 fL, which means that for a sample concentration of 1 nM only 0.06 molecule is inside the detection volume.

The major focus in our laboratory is two-photon microscopy, which proves to be a powerful method in studying both protein oligomerization and cellular processes. Two-photon excitation is the simultaneous absorption of two photons (usually of the same energy) by a molecule that is normally excited by a single photon with twice the energy (45–47). For example, a fluorophore can reach the excited state either by absorption of a single 400-nm photon or by absorption of two 800-nm photons. Two-photon excitation has the advantage that the wavelength of the fluorescence and the wavelength of the excitation light are widely separated. The peak of the emission spectrum for typical fluorophores lies between 450 and 650 nm for excitation at 800 nm; the Raman scattering occurs above 800 nm with a relatively low cross section due to the $1/\lambda^4$ dependence. This makes it easy to separate the fluorescence emission from the excitation light and Raman scattering. Very broad bandpass filters allow the collection of photons across the fluorescence spectrum with high rejection of scattered laser light, thereby improving the sensitivity of fluorescence fluctuation measurements significantly.

The main advantage, however, of two-photon excitation is its inherent optical sectioning effect. The high photon flux required for two-photon excitation occurs only at the microscope focus. Hence the optical arrangement is, when compared with confocal microscopy, straightforward. Due to the localization of molecular excitation, two-photon microscopy ensures that no photodamage results outside the excitation volume.

The number of photon pairs absorbed per fluorophore per laser pulse, n_a, is given by (47)

$$n_a = \frac{\delta \bar{P}^2}{F_P^2 \tau_P^1} \left(\frac{\pi \mathrm{N.A.}^2}{hc\lambda} \right)^2 . \qquad [4]$$

The efficiency of two-photon absorption depends therefore linearly on the two-photon cross section δ and quadratically on the average power $\bar{P}$. The probability of the two-photon absorption depends furthermore on the fourth power of the numerical aperture *N.A.* of the objective, is inversely proportional to the pulse width τ_p, and quadratically inversely proportional to the repetition frequency F_p.

Fluorescence fluctuation experiments are performed on samples at very low concentrations (in the range from picomolar to micromolar). In consequence, it is important to maximize the detected photon counts per molecule to achieve good signal-to-noise ratios. There-

fore, to carry out successful fluorescence fluctuation measurements it is of utmost importance to have an efficient two-photon setup. Each parameter that determines the two-photon absorption should be optimized. The general instrument setup for two-photon fluorescence fluctuation spectroscopy used in this contribution is shown in Fig. 2. The setup is based on the instrument described by Berland (48).

2.2. Instrument Setup

2.2.1. Laser

The pulse width and repetition frequency of the laser are determining factors for the efficiency of the two-photon process (see Eq. [4]). At the same average power, a short pulse width ensures higher instantaneous power and a more effective two-photon excitation compared with a longer pulse width. We use a Ti:sapphire laser (Mira 900, Coherent Inc., Santa Clara, CA) in this work. The pulse width of the laser is ~100 fs under optimal conditions. This ultrashort laser pulse is susceptible to pulse broadening caused by chromatic dispersion of glass materials, such as objectives, lens elements, and polarizers. The final pulse width of the laser at the sample is estimated to be on the order of 150 fs. The repetition rate of the laser is 80 MHz. The gain medium of the system, the titanium: sapphire crystal, will lase over the wavelength range from 690 to 1000 nm.

2.2.2. Detector Considerations: PMT versus APD

The photon counting mode is the ultimate choice for fluorescence fluctuation experiments, where there are always very few molecules inside the excitation volume, and where the number of detected photons is limited. Two types of detectors have been used in this work, a photomultiplier tube (PMT) R-5600 (Hamamatsu, Japan) and an avalanche photodiode (APD) (EG&G, Canada). Both detectors have low dark counts, high gain, and a fast response time, and are optimized for single photon counting.

Figure 3 compares the quantum efficiency of the PMT and the APD. The R-5600 photocathode consists of alkali metals. The APD, on the other hand, uses a different physical principle than the PMT to detect photons. The quantum efficiency of the APD is for wavelengths above 450 nm higher than the efficiency of the PMT and has a maximum of 70% at about 700 nm. One disadvantage of the APD is its very small active area (about 180 μm in diameter).

2.2.3. Data Acquisition

A newly designed data acquisition card stores all detected photon counts in computer memory. This mode of operation provides a record of the experiment similar to that discussed in the introduction. As we have seen in regard to the original fluctuation data of Svedberg and Inouye, we still need to apply statistical

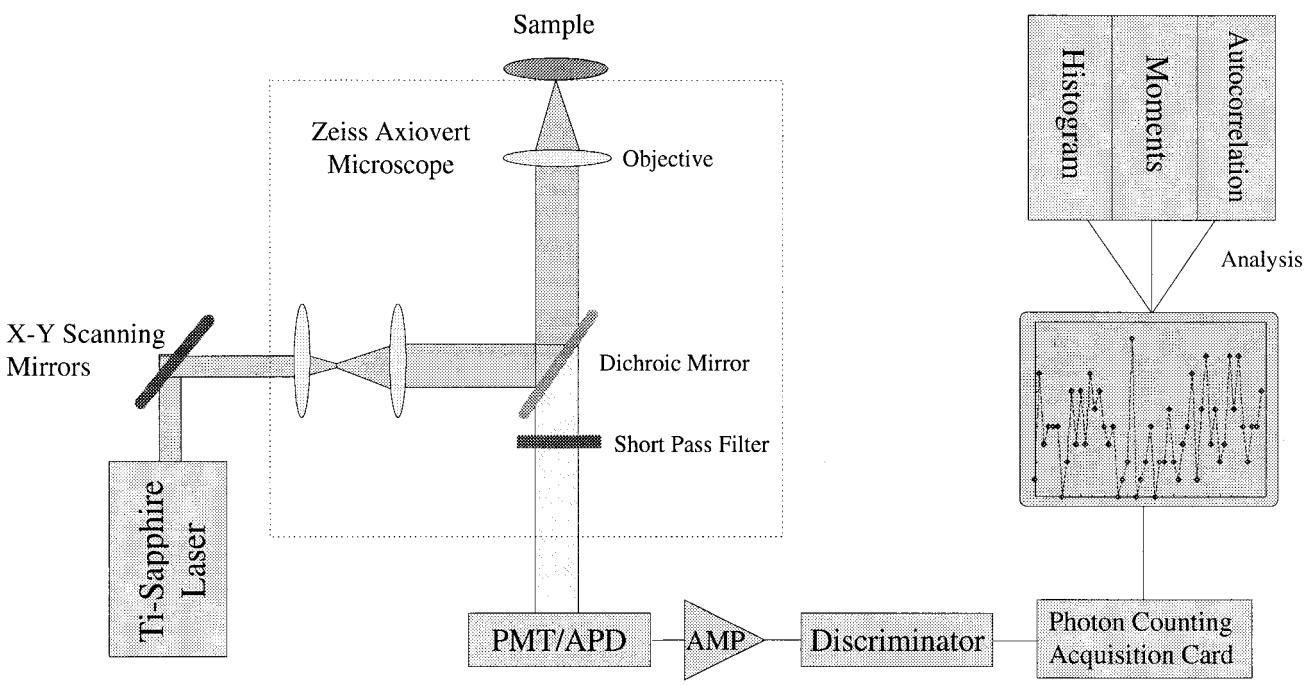

FIG. 2. Schematic of two-photon FFS instruments. The mode-locked Ti-sapphire laser provides an efficient two-photon excitation light source. The excitation light is send to the Zeiss microscope. Either a PMT or an APD detects the fluorescence generated by the two-photon excitation. Finally, the photon counts from the photon counting module are saved on the computer hard disk, and are analyzed later by different methods.

tools to reduce the data into an intelligible form, but the complete history of the photon count events is available for analysis. The data reduction is performed by software and is thus very flexible. The autocorrelation function can, of course, be obtained directly from the data, and a simple change of the software algorithm allows the determination of higher-order autocorrelation. PCH and moment analysis can also be easily performed on the same data record.

2.2.4. Microscope, Optics, and Electronics

The experiments were carried out with either a Zeiss Axiovert 35 or a Zeiss Axiovert 135 TV microscope. The Zeiss Axiovert 135 TV has a detector port directly underneath the emission tube lens, with a twofold increase in the photon collection efficiency compared with the Zeiss Axiovert 35. For all the measurements presented in this contribution, the excitation wavelength was in the range 770 to 790 nm. The power at the sample ranged from 100 μW to 50 mW depending on the experiment. The dichroic mirror (650DCSP, Chroma Technology, Brattleboro, VT) reflects the laser excitation very well from 650 to 850 nm, and transmits 90% of the fluorescence from 400 to 625 nm. Glass filters, either BG-39, BGG-22, or CM-500 (Chroma Technology, Brattleboro, VT), were used as emission filters to eliminate the remaining excitation light.

The photon counting module consists of a photon detector, preamplifer, discriminator, and homebuilt computer acquisition card. For the PMT, the signal is first amplified (Phillips Scientific, Model 6931, Ramsey, NJ) and then converted to TTL pulses with a discriminator (Phillips Scientific, Model 6930). The APD detector, preamplifer, and discriminator are built into a single unit. The photon counts are fed into the acquisition card and sampled with a variable time resolution from 0.1 μs to 1 ms. The recorded photon counts as a function of time are saved to a data file in the acquisition computer and analyzed later with either PV-WAVE Version 6.10 (Visual Numerics, Inc.) or LFD Globals Unlimited software (Champaign, IL).

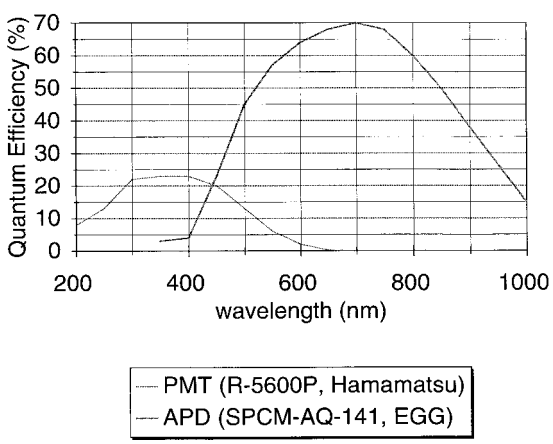

FIG. 3. Comparison of quantum efficiency of APD (SPCM-AQ-141, EGG) and PMT (R-5600P, Hamamatsu).

2.2.5. Fluorophores

The one-photon absorption cross section of a molecule is typically on the order of 10^{-16} to 10^{-17} cm^2. The two-photon absorption cross section, on the other hand, depends on the lifetime of the intermediate state, and is approximately on the order 10^{-49} cm^{4}s/photon. Two-photon cross sections of several fluorescent dyes have been studied in detail (49–51). The two-photon excitation spectrum is similar to the equivalent one-photon excitation spectrum if the fluorophore has no center of symmetry. However, for several commonly used fluorophores such as fluorescein and rhodamine B, the excitation spectra are blue shifted compared with the equivalent one-photon wavelength. In consequence, they can be very well excited at, e.g., 780 nm, where the equivalent one-photon excitation is very poor. Most blue dyes, such as cascade blue and coumarin-based dyes, maintain their equivalent one-photon excitation spectra, and can be excited at 780 nm as well. Using a single wavelength for two-photon excitation provides tremendous flexibility for fluorescence fluctuation measurements; no change in optics is necessary for measuring a "blue" dye or a "red" dye. The fluorescence property of the probes, on the other hand, does not depend on the wavelength of the one-photon or two-photon excitation, since in general the fluorescence quantum yield is the same for both methods of excitation. Xanthen dyes have in general a good two-photon cross section at 780 nm, a high fluorescence quantum yield, and good photostability; consequently, they have been used for most experiments presented here. The dyes we found to be very useful in fluorescence fluctuation measurements are fluorescein, rhodamine 6G, rhodamine 110, rhodamine 123, cyanohydroxycoumarin, and tetrafluorofluorescein (Molecular Probes, Eugene, OR).

Figure 4 shows the PCH analysis of several dyes excited at 780 nm. The APD was used as detector. Rhodamine 110 and rhodamine 123 are pH insensitive from pH 3 to 9; they have spectral properties very similar (both absorption and emission) to those of fluorescein at basic pH, but give almost two times more counts per second per molecule (*cpsm*) than fluorescein. Rhodamine 6G, on the other hand, has a higher quantum yield in ethanol than in water; we obtained 121,000 *cpsm* with moderate excitation power (21 mW at the sample) with two-photon excitation.

2.3. Special Considerations for Sample Preparations

For biological applications, the amount of sample available is often very limited. It is advantageous to reduce the volume and the concentration of a sample

used in the measurements. In a typical two-photon fluorescence fluctuation experiment, the excitation volume is on the order of 10^{-1} μm^3. Compared with the excitation volume of typically 10^9 μm^3 for conventional fluorescence cuvette experiments, the two-photon excitation volume is 10 orders of magnitude smaller. The sample concentrations typically used in fluorescence fluctuation measurements range from micromolar to picomolar. It therefore seems possible to perform fluorescence fluctuation measurements on a few microliters of a highly diluted sample. Unfortunately, there are some experimental complications that might occur and disturb the measurements.

The adsorption of a small amount of sample to the sample holder results in a concentration change. This is especially important for large surface-to-volume ratios and low concentrations, which can lead to a significant fraction of adsorbed sample at the container walls. Therefore, a small surface-to-volume ratio is preferred for fluorescence fluctuation experiments.

3. PHOTON COUNTING HISTOGRAM

3.1. Overview

Traditionally, the analysis of the time sequence of the fluorescence fluctuation experiment provides the number of fluorescent particles in a small volume and the autocorrelation time of the fluctuation, i.e., the average permanence time of the number fluctuation. We recently demonstrated that photon counting histogram (PCH) analysis constitutes a novel tool to extract quantities from fluorescence fluctuation data (1). For example, if we have two molecules with the same translational diffusion coefficient but of substantial difference in brightness, the autocorrelation analysis is unable to provide the distribution of fluorescence intensity, while the PCH analysis can resolve the distribution of molecular brightness. We note that the contrast given by the difference in brightness is frequently larger than the contrast based on translational diffu-

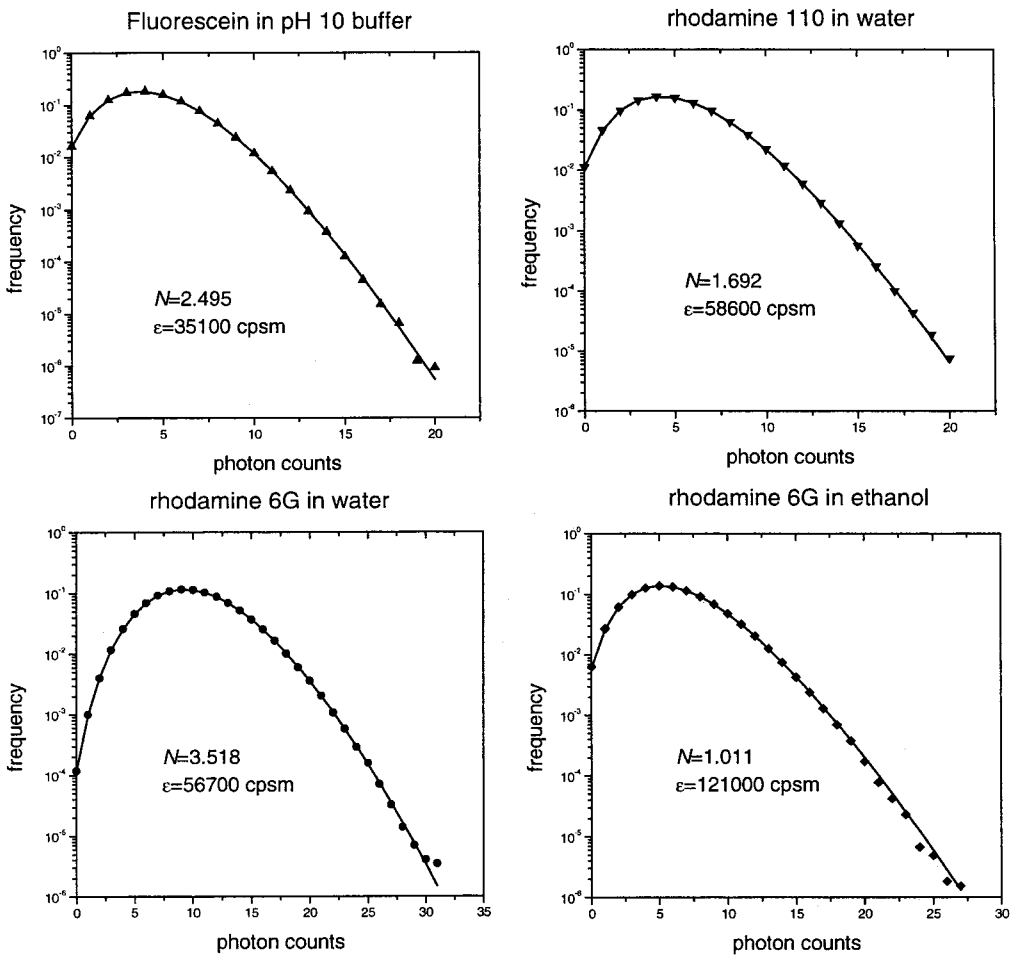

FIG. 4. Comparisons of several common dyes used in two-photon fluorescence fluctuation experiments. All the samples have been measured under identical conditions: excitation at 780 nm, emission bandpass filter CM-500, APD as detector, and with 21 mW of power at the sample. Fluorescein is dissolved in pH 10 Tris buffer; rhodamine 110 is measured in water. We also compared rhodamine 6G in water and ethanol. The counts per second per molecule increases by a factor of 2 when rhodamine 6G is dissolved in ethanol instead of water.

sion. In fact, the translational diffusion scales with the cubic root of the molecular weight, so that a factor of 2 in the diffusion coefficient corresponds to a factor of 8 in the mass. In this contribution we do not derive the basic equations but the interested reader can find them in Chen *et al.* (1).

3.2. Experimental PCH

3.2.1. PCH of Fluorophores at Different Concentrations

The detected photon counts of a constant intensity light source are Poissonian distributed. The concentration fluctuations of a small volume are also governed by Poissonian statistics; therefore, one might first naively expect that the photon counts of diffusing particles will also follow a Poisson distribution. In Fig. 5 the experimentally determined PCHs of the dye fluorescein are shown for three different concentrations in a semilogarithmic plot. The Poisson distribution with a mean equal to the experimental average counts $\langle k \rangle$ is displayed for each histogram as a solid line. The recorded PCH for a dye concentration of 550 nM (Fig. 5A) reaches almost 60 counts per sampling period with an average of $\langle k \rangle \approx 26$ counts. A Poisson distribution with the same average as the experimental photon counts approximates the data. However, decreasing the dye concentration yields PCHs that are not described by Poisson statistics. At a fluorescein concentration of 55 nM (Fig. 5B) a broadening of the experimental PCH compared with the Poisson distribution is observed. The deviation is clearly visible at the tail of the distribution, which corresponds to high photon counts. The deviation of the PCH from the Poisson distribution becomes even more apparent by reducing the fluorescein concentration to 5.5 nM (Fig. 5C).

Each histogram is also displayed as an inset in Fig. 5 using a linear scale. In this representation no deviation between the experimental data and a Poisson distribution is detectable by visible inspection. Since each histogram is based on more than 10^6 data points, the histogram values of the PCH can span six orders of magnitude. A logarithmic scale for the histogram values is therefore essential to pick up the deviations from a Poisson distribution.

In the next step we take the same experimental data sets and model them using the PCH for a Gaussian–Lorentzian beam profile as explained in Chen *et al.* (1). The corresponding PCH can then be determined by using a fitting algorithm. Each histogram for a single species is characterized by two parameters: the average number of particles $\bar{N}$ in the volume V_{PSF} of the PSF and the average molecular brightness ϵ. The three data sets were recorded under the same conditions, except that the fluorescein concentration was varied. Therefore the average counts per particle ϵ are the same for all three experiments. We performed a global fit of all three histograms with ϵ linked together across all data sets, while the average number of particles was allowed to vary. The data and the fitted histograms for the three different concentrations in Fig. 6 are in good agreement. The residuals between data and fit for each histogram are displayed in Fig. 6 with each unit representing the standard deviation σ. The residuals are random across the counts k and the reduced X^2 is close to 1, indicating a good description of the data by the theoretical model. The fit parameters and the average counts are compiled in Table 1. The recovered number of molecules $\bar{N}$ scales exactly with the average photon counts $\langle k \rangle$ as predicted by the theory. However, the ratio of both parameters for each successive dilution is 9.7 instead of 10 as expected for the dilution experiment, thus suggesting an overestimation of the experimental dilution factor.

3.2.2. PCH of Fluorophores with Different Brightness

We used three different fluorophores, each with its own brightness parameter ϵ, to illustrate the influence of the molecular brightness ϵ on the photon count distribution. To facilitate the comparison of the different histograms the concentrations of all of the fluorophores were kept equal. The count distributions were analyzed with the PCH algorithm and are shown together with the fits in Fig. 7. In addition, Poisson distributions with the same mean as the average photon counts are displayed as dashed lines for each histogram. The deviation between the tail of the PCH and the Poisson distribution enhances with increasing ϵ, while for ϵ approaching zero the histogram converges to a Poisson distribution.

3.2.3. PCH of Mixtures

To demonstrate that the PCH of a mixture of two fluorescent species is given by the convolution of the individual histograms the following experiment was carried out. First the PCH distributions of fluorescein and cyanohydroxycoumarin, each at a concentration of 1.2 nM, were obtained separately. In the next step fluorescein and cyanohydroxycoumarin were mixed together, so that the concentration of each dye remained unchanged. The photon count distribution of the mixture was measured and is well represented by the convolution of the single species histograms as shown in Fig. 8.

3.3. Discussion

Three sources of fluctuations account for the shape of the photon counting histogram. The first one is a consequence of the quantum nature of the detection process. Since the absorption of a photon occurs almost instantaneously, no correlation between the atomic detector system and the electric field for adjacent photon counts exists. This noise generated by the detector is

also known as shot noise and leads to a Poisson distribution of photon counts. The fluctuations of the fluorescent light intensity are caused by the diffusion of molecules in an inhomogeneous excitation profile and the particle number fluctuations within the observation volume, which represent the other two sources of noise. These intensity fluctuations introduce correlations between photon counts and are responsible for the super-Poissonian statistics of the photon count distribution. FCS experiments always measure small, open volumes that freely exchange particles with the surrounding bath. The resulting number fluctuations of such a system alone are sufficient to cause non-Poissonian statistics. As an example, consider a homo-

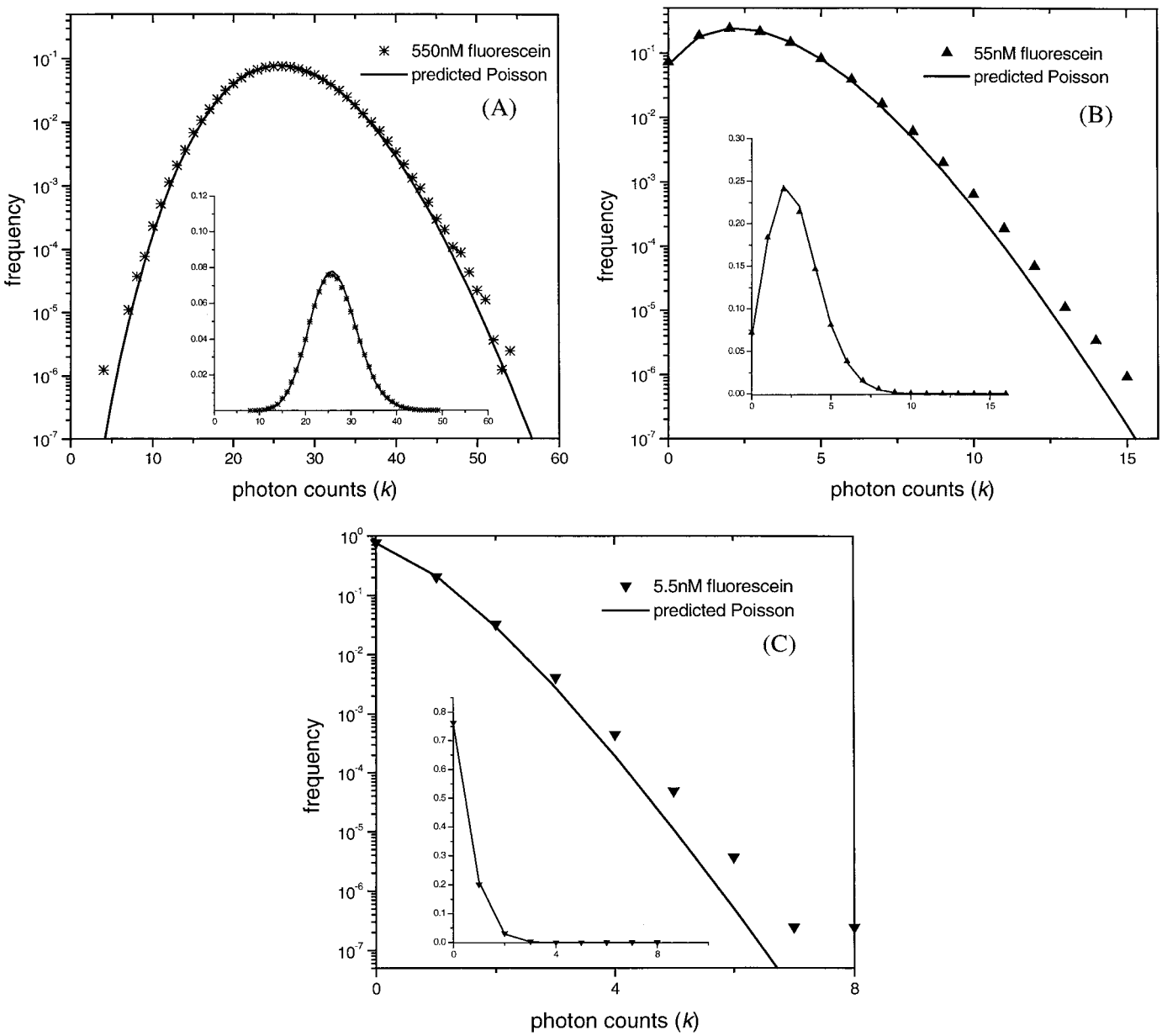

FIG. 5. Comparison of the photon counting histogram for fluorescein at different concentrations with the Poisson distribution. Fluorescein was dissolved in 75% glycerol/25% Tris buffer solution (v/v). The samples were measure with a 63× Plan Apochromat objective (N.A. = 1.4) and an incident laser power at the sample of approximately 7 mW. The histograms for fluorescein at concentrations of (A) 550 nM, (B) 55 nM, and (C) 5.5 nM are plotted together with their Poisson distributions for a mean equal to the corresponding average photon counts $\langle k \rangle$ of the experimental histogram (Table 1). For the highest concentration only small deviations from a Poisson distribution are noticeable. Lowering the concentration of the fluorescein results in increased deviations of the histogram from a Poisson distribution as shown in (B) and (C). This deviation of the experimental data from the Poisson distribution is much more pronounced in the logarithmic representation as compared with the linear scale (shown in the inset).

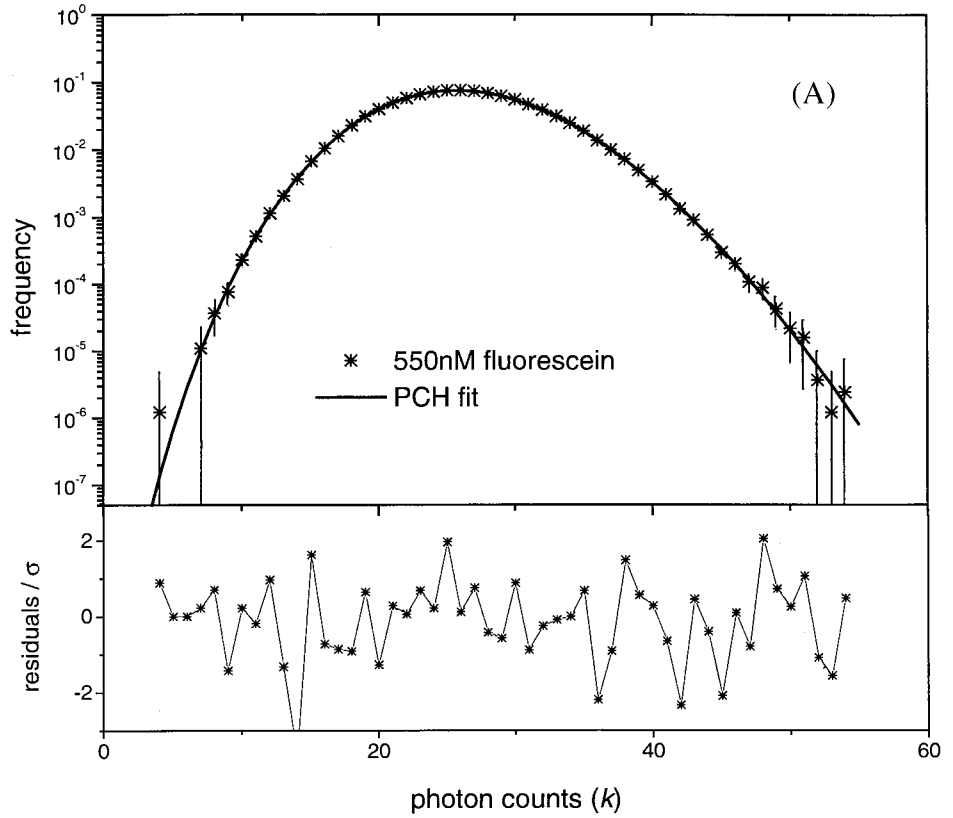
(A)
frequency
550nM fluorescein
PCH fit
residuals / σ
photon counts (k)

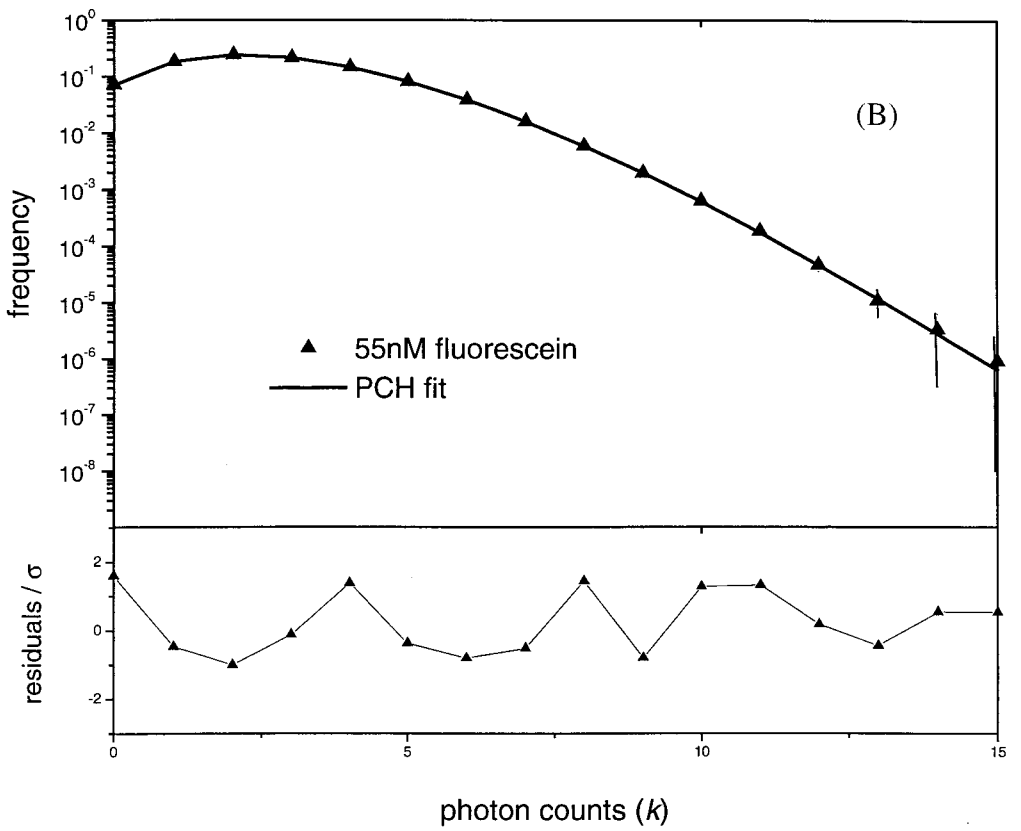
(B)
frequency
55nM fluorescein
PCH fit
residuals / σ
photon counts (k)

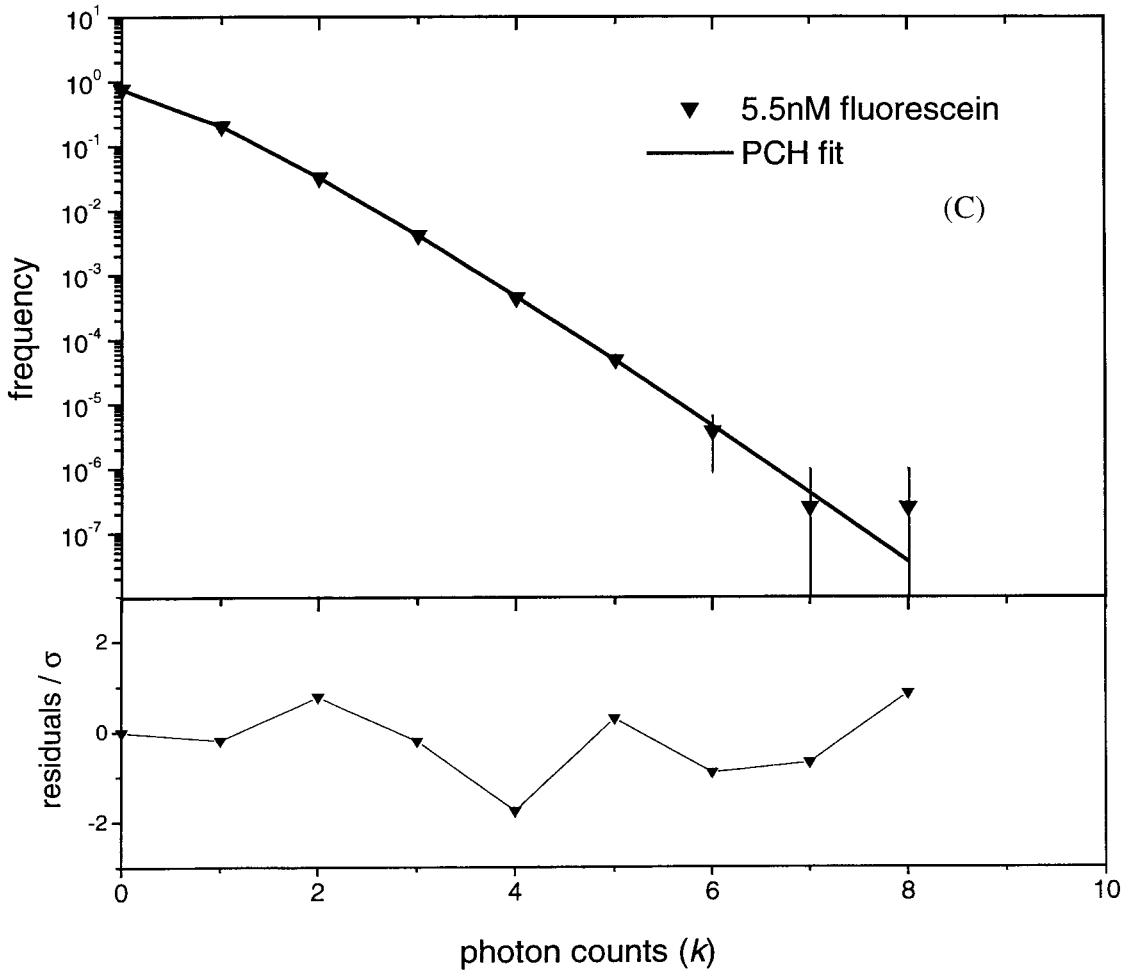

FIG. 6—*Continued*

geneous excitation profile, where the fluorescence intensity is not affected by the diffusion inside the observation volume. In this case the particle fluctuations lead to a compound Poisson distribution of photon counts. The fact that the count distribution follows super-Poissonian instead of Poissonian statistics is crucial to extract information from the histogram. Instead of one parameter, which is sufficient to characterize a Poisson distribution, two parameters, the average number of molecules in the excitation volume $\bar{N}$ and the brightness coefficient ϵ, are required to uniquely describe the single-species histogram. The deviation of the PCH from a Poisson function is most pronounced in the tail of the distribution. Since the histogram values span several orders of magnitude, a logarithmic data representation as illustrated in Fig. 5 is necessary to make the super-Poissonian character of the PCH visible.

The photon counting histogram approaches a Poisson distribution with increasing fluorophore concentration as shown in Fig. 5. This behavior can be readily understood by considering the influence of the molecule concentration on the intensity fluctuations. The relative strength of the number fluctuations is given by

FIG. 6. Photon counting histogram for fluorescein at three different concentrations: (A) 550 nM, (B) 55 nM, and (C) 5.5 nM. The same histograms as used in Fig. 5 are plotted as symbols together with an error bar ($\pm 3\sigma$) for each data point on a semilogarithmic scale. The three data sets were fit by globally linking the molecular brightness parameter ϵ across the data sets, while allowing the average number of molecules $\bar{N}$ to vary. The solid line represents the best fit obtained by using the theoretical PCH function $\Pi(k; \bar{N}, \epsilon)$. The fitting parameters are compiled in Table 1. The lower panel displays the normalized residuals of the fit. The reduced X^2 for each individual data set is shown in the table with a global X^2 of 1.01. The average number of photon counts per sampling period $\langle k \rangle$ was calculated directly from the experimental data. The ratios of the concentration, the photon counts $\langle k \rangle$, and the number of molecules $\bar{N}$ were determined relative to the lowest concentration case.

the ratio between the standard deviation σ and the mean μ of the molecule distribution,

$$\frac{\sigma}{\mu} = \frac{\sqrt{\langle \Delta N^2 \rangle}}{\bar{N}} = \frac{1}{\sqrt{\bar{N}}}, \quad [5]$$

and characterizes the relative width of the distribution. The number of molecules inside a small, open volume is Poisson distributed, and the relative strength of the particle fluctuations decreases with the inverse square root of the average number of particles $\bar{N}$. Thus with increasing particle concentration the number distribution approaches a delta function $\delta(N - \bar{N})$. Consequently the intensity fluctuations associated with the particle number die away. The second contribution to the intensity fluctuations, due to the diffusion in an inhomogeneous excitation profile, also vanishes at high particle concentrations; a vacancy created by a molecule leaving a position is almost always filled by another molecule moving to that position, so that no net change in the fluorescence intensity occurs. Thus the constant fluorescence intensity dictates a Poissonian photon count distribution.

To maximize the deviation between the photon count distribution and the corresponding Poisson function, one can either reduce the number of molecules within the excitation volume or increase the brightness parameter ϵ as demonstrated in Fig. 7. The relationship between the super-Poissonian character of the PCH and the molecular brightness ϵ can be qualitatively understood. The average fluorescence intensity of a molecule in the excitation volume is characterized by the parameter ϵ. A particle with a larger value of ϵ causes stronger intensity fluctuations as it enters and diffuses through the beam. The increase in the fluorescence intensity fluctuations leads to a further broadening of the PCH. To quantify this statement, we define the fractional deviation Q, a measure of the deviation between the PCH and the Poisson distribution (52),

$$Q = \frac{\langle \Delta k^2 \rangle - \langle k \rangle}{\langle k \rangle} = \gamma\epsilon \quad [6]$$

where $\langle \Delta k^2 \rangle$ and $\langle k \rangle$ are the variance and the expectation value of the photon counts, respectively. A Poissonian distribution is defined by $Q = 0$, while super-Poissonian distributions require $Q > 0$ and sub-Poissonian distributions mandate $Q < 0$. Q is directly proportional to the molecular brightness ϵ and the shape factor γ of the PSF. The γ factor is constant for a given PSF. Thus the super-Poissonian character of PCH is determined largely by ϵ, which varies with the excitation power, the detection quantum yield, and the molecular species.

Generalization to more than one species has been described by Chen *et al.* (1). The PCH of a two species sample is the convolution of the individual photon count distributions. Thus four parameters, the average number of molecules and the brightness of both species, are required to characterize the photon count distribution completely. The molecular brightness ϵ and the average number of molecules $\bar{N}$ shape the histogram distinctively as discussed earlier. The convolution will change, but still preserve the characteristics of each individual species. Thus as long as there is a brightness difference between the species, PCH could resolve them regardless of their diffusion coefficient.

3.4. Simulation of a Monomer–Dimer Mixture

We recently resolved mixtures of dyes experimentally (53). However, here we look at a simple simulation of an oligomer mixture to better illustrate the potential of PCH. Let us consider a monomer–dimer mixture, where each monomeric unit is labeled with a fluorescent marker. If there is no quenching occurring on association, the dimers appear as a species with twice the molecular brightness compared with the monomers, since each dimer carries two fluorescent labels. We simulate this scenario for a monomer con-

TABLE 1

PCH Analysis of a Fluorescein Dilution Experiment[a]

c (nM)	$\frac{c}{[5.5\text{nM}]}$	$\langle k \rangle$	$\frac{\langle k \rangle}{0.28}$	ϵ	$\bar{N}$	$\frac{\bar{N}}{0.347}$	Reduced X^2
550	100	26.25	93.8	0.807	32.53	93.7	1.14
55	10	2.71	9.7	0.807	3.36	9.7	0.98
5.5	1	0.28	1.0	0.807	0.347	1.0	0.84

[a] The photon counting histogram of fluorescein for three different concentration was fitted globally to the theoretical PCH function $\Pi(k; \bar{N}, \epsilon)$. The molecular brightness ϵ was linked across the data sets, while the average number of molecules $\bar{N}$ was allowed to vary. The reduced X^2 for each individual data set is shown in the table with a global X^2 of 1.01. The average number of photon counts per sampling period $\langle k \rangle$ was calculated directly from the experimental data. The ratios of the concentrations, the photon counts $\langle k \rangle$, and the number of molecules $\bar{N}$ were determined relative to the lowest concentration case.

centration of 1.0 nM and a dimer concentration of 0.2 nM with an excitation volume of 1.2 fL. We chose a molecular brightness of the monomeric unit of 49,000 cpsm, a sampling interval of 50 μs, and a data acquisition time of 10 min.

By using the theory we calculated the corresponding photon counting histogram and added statistical noise to the data to make the simulation realistic. The histogram of the photon counts (Fig. 9A) was first fit with a single species model and then subject to a two-species model. The residuals of the single-species fit are displayed in Fig. 9B together with the residuals of the two-species fit. A single-species model clearly fails to describe the data accurately. The residuals are correlated and yield a reduced X^2 of 14, while the residuals of the two species model are random and lead to a reduced X^2 close to one. The parameters recovered by the fit are specified in the figure legend and are in good agreement with the simulation parameters.

The major advantage of the PCH technique is its ability to resolve different species in a single measurement. In contrast the $G(0)$ analysis, which we introduce later in this text, yields a single value for each measurement and therefore cannot resolve two species in a single measurement.

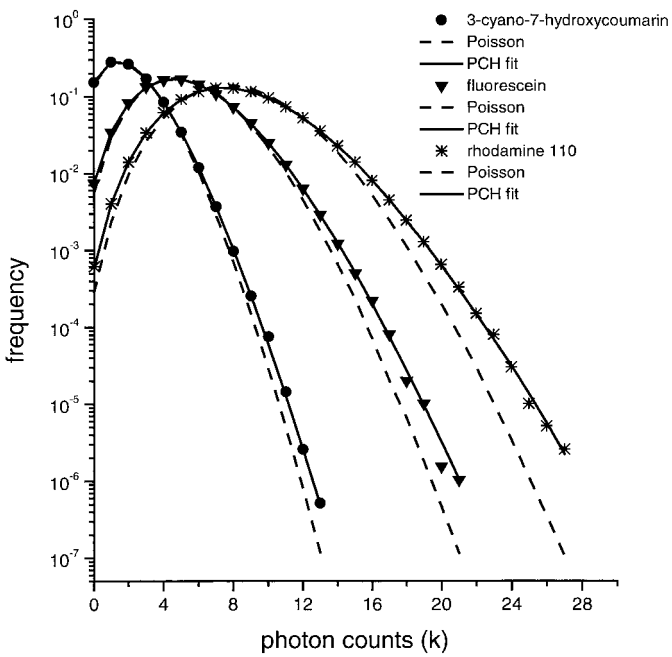

FIG. 7. Photon counting histograms for three dyes differing in their molecular brightness ϵ. The fit recovered the average number of molecules $\bar{N}$ as 2.6, 3.3, and 3.0 for cyanohydroxycoumarin, fluorescein, and rhodamine 110, respectively. A molecular brightness ϵ with values of 0.738 for cyanohydroxycoumarin, 1.60 for fluorescein, and 2.73 for rhodamine 110. For each histogram a Poisson distribution with a mean equal to the average number of photon counts is plotted as a dashed line.

4. FLUORESCENCE CORRELATION SPECTROSCOPY

Two fundamental physical properties can be determined from the autocorrelation function, $G(\tau)$ [for a review, see (41)]: (1) the kinetic information, which is characterized by the decay of the autocorrelation function (13, 16, 18, 24, 54); (2) the fluctuation amplitude of $G(\tau)$ at $\tau = 0$, $G(0)$, which characterizes the strength of the fluctuation signal and is given by the normalized variance of the fluorescence intensity, $\langle \Delta F^2 \rangle / \langle F \rangle^2$ (33, 38, 55).

4.1. G(0) Analysis

4.1.1. G(0) of a Single Species

For a single fluorescent species, the time-zero value of the autocorrelation function, $G(0)$, depends on the average number of molecules inside the excitation volume,

$$G(0) = \frac{\langle F^2 \rangle - \langle F \rangle^2}{\langle F \rangle^2} = \frac{\gamma}{\langle N \rangle}, \qquad [7]$$

where γ is a geometric factor and depends only on the shape of the excitation volume,

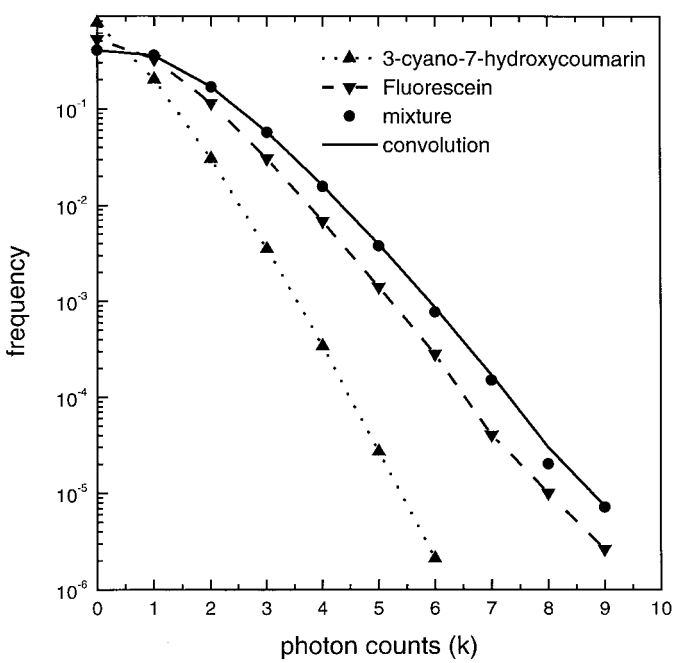

FIG. 8. Photon counting histogram for fluorescein at 1.2 nM (▼), cyanohydroxycoumarin at 1.2 nM (▲), and the mixture of fluorescein and cyanohydroxycoumarin (●) each at a concentration of 1.2 nM. The solid line was determined by convoluting the experimental histograms of the individual dyes (dashed lines to guide the eye) and matches the photon counting histogram of the mixture.

$$\gamma = w_2/w_1, \quad [8]$$

with the constant w_n defined as,

$$w_n = \int [I^2(r)/I^2(0)]^n d^3r. \quad [9]$$

The geometric factor γ is equal to $\frac{3}{4}\pi^2$ (0.07599) for the Gaussian–Lorentzian PSF and equal to $\frac{1}{2}\sqrt{2}$ (0.3535) for the 3D Gaussian PSF.

The experimental observable in a fluorescence fluctuation experiment is not the fluorescence intensity, but the photon counts. The $G(0)$ value contains the shot noise contribution of photon counts. A direct calculation of $G(0)$ based on the photon counts according to Eq. [7] leads to an overestimation of $G(0)$. Two approaches have been applied to recover the "true" $G(0)$ value without the shot noise contribution of the photon counts:

1. A straightforward way is to extrapolate $G(0)$ from $G(\tau)$ at $\tau \neq 0$ (33, 56). Detectors have no memory of the photons detected in the past because the absorption process is almost instantaneous. Thus, there is no shot noise contribution at any other channels except at $\tau = 0$. The extrapolation of $G(0)$ obtained by fitting to the appropriate model relies on the knowledge of the underlying kinetic processes that contribute to the intensity autocorrelation function. Hence, it is necessary to develop physical models to describe and account for these kinetic processes.

2. The second approach is called scanning FCS (S-FCS) and was introduced by Weissman *et al.* (57) to determine molecular weight of DNA samples labeled with ethidium bromide. This method requires a periodic spatial sampling of the probe with a time period T. If the diffusion is negligible within the first period T, then $G(T)$ will be equivalent to the ideal $G(0)$ without shot noise contributions. The merits of this method are to measure multiple independent excitation volumes simultaneously and to eliminate background contributions to the autocorrelation function. The signal-to-noise ratio increases significantly when measuring molecules with slow diffusion. S-FCS has been successfully implemented to investigate several types of oligomer dissociation (43), and it has been used to determine the diffusion coefficients of biopolymers and the number of particles in biological systems (17, 58).

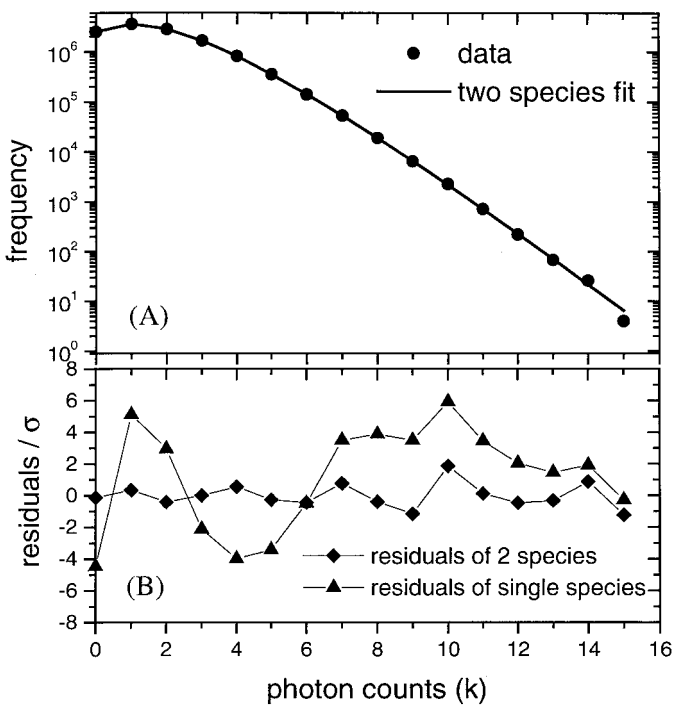

FIG. 9. Simulated photon counting histogram for a monomer–dimer mixture as explained in the text. The concentrations of monomers and dimers are 1.0 and 0.2 nM, respectively. Monomers contribute a molecular brightness ϵ of 49,000 cpsm, while the dimers are twice as bright. (A) The histogram together with a fit to a two-species model. (B) The residuals of the two-species fit yield a reduced X^2 of 1. The fit recovered a concentration of 1.0 nM and a molecular brightness of 48,000 cpsm for the monomer species. For the dimer species a concentration of 0.21 nM and a molecular brightness of 99,000 cpsm were retrieved. A fit of the histogram to a single-species model was poor, with a reduced X^2 of 14 and nonrandom residuals.

4.1.2. G(0) of Two Species

The $G(0)$ value for multiple species is the sum of all single-species $G(0)$ values weighted by the square of the fractional intensity (41). For two species, A and B, the resulting value of $G(0)$ can be expressed in terms of the average number of molecules, $\bar{N}_A$ and $\bar{N}_B$, and the molecular brightness, ϵ_A and ϵ_B:

$$G(0) = \gamma \frac{\epsilon_A^2 \bar{N}_A + \epsilon_B^2 \bar{N}_B}{(\epsilon_A \bar{N}_A + \epsilon_B \bar{N}_B)^2}. \quad [10]$$

If the brightnesses of the two species are identical, Eq. [10] reduces to the single-species case, and $G(0)$ represents again the total number of molecules $\bar{N}$. When the brightnesses ϵ of the two-species differ, $G(0)$ does not reflect the total number of molecules, but depends on the brightness and the population of the individual species. Since $G(0)$ represents only a single value no discrimination between species is possible without further knowledge. However, if the two species are coupled by a binding equilibrium, then it is possible to establish the link between $G(0)$ and the individual species by performing a titration experiment. The resulting $G(0)$ values can then be evaluated by fitting to a model.

4.2. Translational Diffusion

The temporal decay of the autocorrelation function, $G(\tau)$, contains information about the dynamics of the

system. Depending on the time scale of interest, one can observe fluorescence lifetimes, triplet state reactions, and rotational and translational diffusion (13, 59–61). The dynamic information contained in FCS is often overwhelming.

4.3. Practical Issues

4.3.1. Calibration of the Excitation Volume

To convert the experimentally recovered $G(0)$ into a concentration for the chemical species of interest, the size of the excitation volume must be determined for a given instrumental setup. The beam profile of the laser, the alignment of the microscope optics, and the maintenance of the exterior optics influence the size of the excitation volume. Variations in the excitation volume by a factor of 2 can occur (48). To calibrate the excitation volume, we often perform an experiment with a sample of known concentration and of known diffusion coefficient. Experimentally, we do not measure diffusion coefficients directly, but we measure the residence time of a molecule inside the excitation volume given by $w_0^2/8D$. To recover the excitation volume from the residence time of the molecule, the diffusion coefficient must be obtained by other methods. In the past, fluorescent spheres of known diameter were used for calibration. However, spheres tend to aggregate as a function of time. Depending on the size and the concentration of the spheres, they aggregate on the time scale of minutes to hours. Furthermore, spheres also adsorb to many other materials, such as test tubes, glass slides, and biological cells (18). Frequently, the fluorescence intensity from the sphere sample varies during the course of hours due to the adsorption to the sample holder.

All the calibration work presented in this contribution is based on specific fluorescent dyes. Fluorescent dyes are stable and less susceptible to sample preparations. The most commonly used dye is fluorescein in high-pH buffer [50 mM Tris buffer (Sigma, St. Louis, MO), pH 10]. Fluorescein is a pH-sensitive dye, and its spectroscopic properties vary drastically from pH 7.5 to 2. At pH $>$ 7.5, fluorescein has a constant quantum yield (greater than 0.93) and very good water solubility (62). The major benefit of using fluorescein is its lack of interactions with surfaces; consistent results are always obtained regardless of the type of sample holder used. Another frequently used dye is rhodamine 110; rhodamine 110 has lower water solubility than fluorescein, but is, under identical instrumental conditions, almost by a factor of 2 brighter than fluorescein. Fig. 10A shows the autocorrelation curve of 4 nM fluorescein in Tris buffer. Fig. 10B shows the autocorrelation curve of rhodamine 110 at 3 nM in water. A global analysis was performed on the data sets. The diffusion coefficient of fluorescein was fixed at 300 $\mu m^2/s$ (41). The Gaussian–Lorentizan beam waist, w_{GL}, was linked between the two data sets and recovered as 0.319 μm. Consequently, the diffusion coefficient of rhodamine 110 was recovered as 272 $\mu m^2/s$.

4.3.2. Sampling Time

Accurate extrapolations of the autocorrelation function to the origin were especially important in the past when the data acquisition was limited to relatively long sampling times. The corresponding time scale for a 50-μs sampling time is indicated as dashed lines in Fig. 10. The extrapolated $G(0)$ is almost a factor of 2 higher than $G(\tau)$ at $\tau = 50$ μs. If the diffusion coefficient of a chemical species is 300 $\mu m^2/s$, and the beam waist of the excitation volume is 0.4 μm, then the residence time of molecules inside the excitation volume is about 70 μs, which is less than a factor of 2 longer than the sampling time. However, improvements of the data acquisition hardware allow sampling times of less than 1 μs, which is almost two orders of magnitude faster than the residence time. For the data shown in Fig. 10, the time bin was 1 μs. The extrapolated $G(0)$ is less than 10% higher than the next channel, $G(1)$. $G(0)$ can be thus replaced by $G(1)$ at the microsecond binning time. Consequently, for systems governed only by translational diffusion, the extrapolation method becomes less important when the data sampling time is on the microsecond time scale.

In addition to translational diffusion, there are other kinetic processes that contribute to the decay of the autocorrelation function. A well-studied system is the triplet state reaction (27). The triplet lifetime is on the order of microseconds. The molecules in the triplet state become “dark,” and therefore are invisible to the detector on the microsecond time scale. The number of molecules available for singlet state excitation is thus reduced, and the $G(1)$ value is increased.

4.4. FCS Studies of Protein Associations

As mentioned in the introduction, one biological system that we have studied using the fluctuation correlation technique is the association/dissociation equilibrium of protein oligomers. One central problem in studying protein interactions is to measure if a protein sample exhibits aggregation and if so to what extent. FCS can be particularly powerful for this application since measurements are made on an unperturbed equilibrium sample *in vitro,* and can be performed at low concentrations not accessible by other methods. To demonstrate the feasibility of these studies using scanning FCS, we have monitored the dissociation by dilution of glycogen phosphorylase A, a tetramer at high (micromolar) concentrations, which dissociates to an active dimer on dilution (63–65). Glycogen phosphorylase from rabbit muscle was purchased from Sigma. After dialysis, the protein was labeled by incubation overnight with fluorescein isothiocyanate (FITC) in 50

mM Tris buffer (pH 9.0) with small amounts of dithiothreitol (DTT) and EDTA. Free dye was removed with a G-25 Sephadex column. The labeling efficiency was 2 fluorescein labels per monomer of phosphorylase. The preparation was then filtered with 0.2-μm filters to remove any large contaminants. A series of dilutions were prepared, from 1 μM down to 1 nM. Solutions were stored overnight to allow equilibration, and then placed on hanging drop microscope slides for measurements of $G(\tau)$.

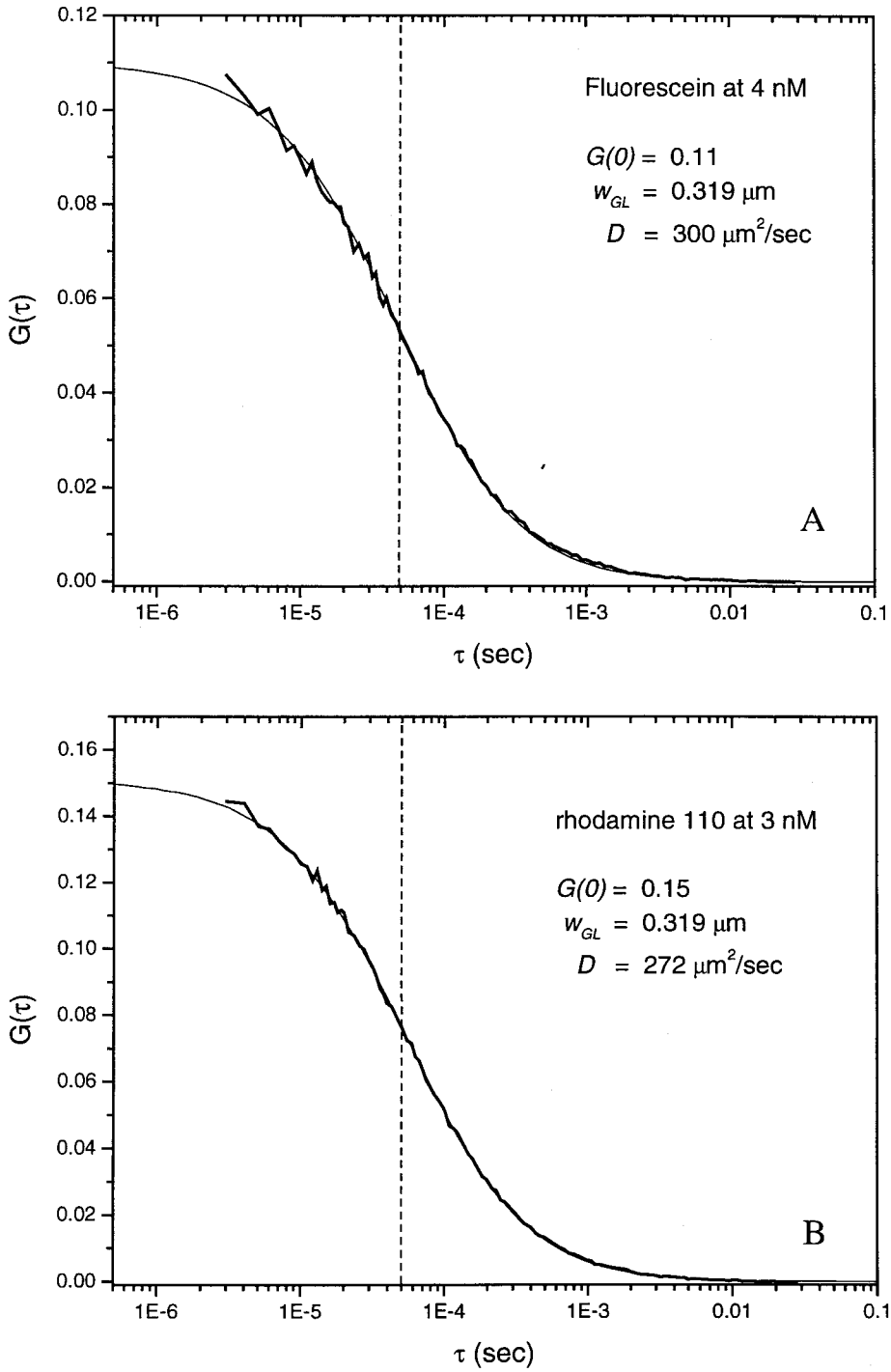

FIG. 10. Autocorrelation curve $G(\tau)$ of two fluorescent dyes, fluorescein (A) and rhodamine 110 (B). The laser power at 780 nm was estimated to be less than 20 mW at the sample. The 40× fluar objective was used for these measurements. The fluorescence was detected by an APD.

If we assume a standard equilibrium relation for the tetramer to dimer protein dissociation,

$$K = \frac{[\mathrm{D}]^2}{[\mathrm{T}]}, \qquad [11]$$

with [D] the dimer and [T] the tetramer concentration, we can calculate the form for $G(0)$ as a function of total protein concentration.

Measurements were made for the different dilutions, and the results are shown in Fig. 11. Though there is significant noise in these measurements, it is clear that the protein dissociates with increasing dilution. The best fit of this data yields $K = 430$ nM (monomer), in good agreement with previous measurements of the dissociation constant (65, 66).

5. SUMMARY

After more than 20 years of development, fluorescence fluctuation spectroscopy is reemerging with exciting new applications in biology and chemistry. The sensitivity provided by fluorescence techniques combined with the extremely small observation volumes achieved by modern microscopy techniques allows the study of biological processes even at the single molecule level. Fluctuations occur spontaneously; thus, kinetic parameters are directly obtained from the analysis of the temporal intensity fluctuations at equilibrium, without perturbing the system.

We illustrate the PCH analysis to characterize the probability distribution of photon counts. PCH and autocorrelation analyses are complementary techniques; PCH exploits the fluctuations in the amplitude domain, while the autocorrelation function uses the same fluctuations in the time domain. We show experimentally that the PCH analysis provides, for the single-species case, the average number of molecules $\bar{N}$ and the molecular brightness ϵ. We generalized the PCH theory to a mixture of species and demonstrated the validity for the case of two species.

The strength of PCH analysis lies in its ability to resolve two species of different molecular brightness in a single experiment. To illustrate this point the simulated photon counting histogram of a monomer–dimer mixture was studied. The analysis of the $G(0)$ value provides an alternative approach to characterize oligomer equilibria, which is based on the change in the average number of molecules in the excitation volume as the proteins oligomerize. We experimentally demonstrated $G(0)$ analysis for a dimer–tetramer equilibrium of proteins. Thus fluorescence fluctuation spectroscopy has matured enough to be considered a viable tool to study protein–protein interactions.

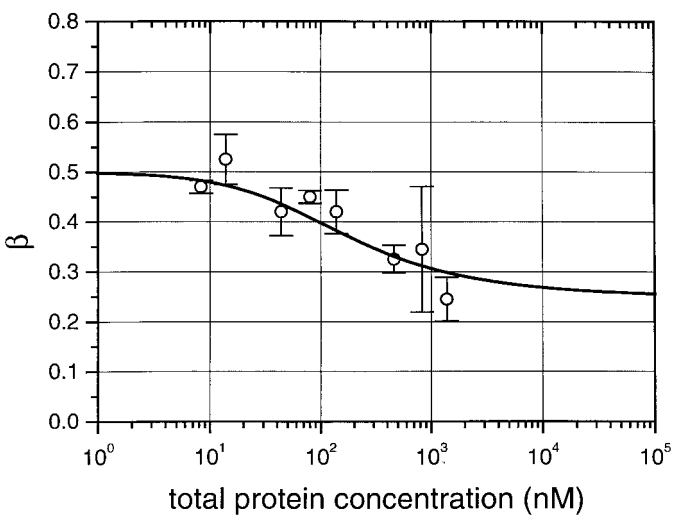

FIG. 11. Dissociation of GPA as it is diluted from micromolar to nanomolar concentration. To directly detect particle aggregation, one can conveniently introduce an association parameter, β, which is a comparison of the fluctuation amplitude measured by FCS with the number of particles expected for a known sample concentration: $\beta \equiv \gamma/G(0) \cdot N_T$, where N_T is the total number of monomer units in the volume. For a monodisperse sample, β will have a value of $1/n$, where n is the number of monomers per particle. Thus, for a tetramer–dimer equilibrium, β will increase from 0.25 to 0.5 as discussed in Berland *et al.* (43).

ACKNOWLEDGMENTS

This work was performed in part under grants from the National Institutes of Health (RR03155) and National Science Foundation (PHY95-13217).

REFERENCES

1. Chen, Y., Müller, J. D., So, P. T. C., and Gratton, E. (1999) *Biophys. J.* **77,** 553–567.
2. Siedentopf, H., and Zsigmondy, R. (1903) *Ann. Phys. [4]* **10,** 1–39.
3. Einstein, A., and von Smoluchowski, M. (1997) Untersuchungen über die Theorie der Brownschen Bewegung, Abhandlung über die Brownsche Bewegung und verwandte Erscheinungen, Verlag Harri Deutsch, Thun/Frankfurt.
4. Svedberg, T., and Inouye, K. (1911) *Z. Phys. Chem.* **77,** 145–191.
5. von Smoluchowski, M. (1914) *Wien Ber.* **123,** 2381–2405.
6. Johnson, J. B. (1928) *Phys. Rev.* **32,** 97–109.
7. Nyquist, H. (1928) *Phys. Rev.* **32,** 110–113.
8. O'Brien, K. P., and Weissman, M. B. (1994) *Phys. Rev. A* **50,** 3446–3452.
9. Weissman, M. B. (1988) *Rev. Mod. Phys.* **60,** 537–571.
10. Luria, S. E., and Delbrück, M. (1943) *Genetics* **28,** 491–511.
11. Weissman, M. B. (1993) *Rev. Mod. Phys.* **65,** 829–839.
12. Bendat, J. S., and Piersol, A. G. (1971) Random Data: Analysis and Measurement Procedures, Wiley–Interscience, New York.

13. Magde, D., Elson, E., and Webb, W. W. (1972) *Phys. Rev. Lett.* **29,** 705–708.
14. Elson, E. L., and Magde, D. (1974) *Biopolymers* **13,** 1–27.
15. Qian, H., and Elson, E. L. (1991) *Appl. Opt.* **30,** 1185–1195.
16. Rigler, R., Mets, U., Widengren, J., and Kask, P. (1993) *Eur. Biophys. J.* **22,** 169–175.
17. Koppel, D. E., Morgan, F., Cowan, A. E., and Carson, J. H. (1994) *Biophys. J.* **66,** 502–507.
18. Berland, K. M., So, P. T. C., and Gratton, E. (1995) *Biophys. J.* **68,** 694–701.
19. Eigen, M., and Rigler, R. (1994) *Proc. Natl. Acad. Sci. USA* **91,** 5740–5747.
20. Rigler, R. (1995) *J. Biotechnol.* **41,** 177–186.
21. Ehrenberg, M., and Rigler, R. (1974) *Chem. Phys.* **4,** 390–401.
22. Aragon, S. R., and Pecora, R. (1975) *Biopolymers* **14,** 119–137.
23. Kask, P., Piksarv, P., Pooga, M., and Mets, Ü. (1989) *Biophys. J.* **55,** 213–220.
24. Koppel, D. E., Axelrod, D., Schlessinger, J., Elson, E. L., and Webb, W. W. (1976) *Biophys. J.* **16,** 1315–1329.
25. Magde, D., Webb, W. W., and Elson, E. L. (1978) *Biopolymers* **17,** 361–376.
26. Magde, D., Elson, E. L., and Webb, W. W. (1974) *Biopolymers* **13,** 29–61.
27. Widengren, J., Mets, U., and Rigler, R. (1995) *J. Phys. Chem.* **99,** 13368–13379.
28. Kinjo, M., and Rigler, R. (1995) *Nucleic Acids Res.* **23,** 1795–1799.
29. Schwille, P., Oehlenschlager, F., and Walter, N. G. (1996) *Biochemistry* **35,** 10182–10193.
30. Borejdo, J. (1979) *Biopolymers* **18,** 2807–2820.
31. Brock, R., Hink, M. A., and Jovin, T. M. (1998) *Biophys. J.* **75,** 2547–2557.
32. Magde, D. (1976) *Q. Rev. Biophys.* **9,** 35–47.
33. Palmer, A. G. d., and Thompson, N. L. (1987) *Biophys. J.* **52,** 257–270.
34. Qian, H., and Elson, E. L. (1989) *in* Applied Polymer Symposia, pp. 305–314, Wiley, New York.
35. Qian, H., and Elson, E. L. (1990) *Proc. Natl. Acad. Sci. USA* **87,** 5479–5483.
36. Saleh, B. (1978) Photoelectron Statistics with Applications to Spectroscopy and Optical Communication, Springer-Verlag, Berlin/New York.
37. Press, W. H., Teukolsky, S. A., Vetterling, W. T., and Flannery, B. P. (1993) Numerical Recipes in C: The Art of Scientific Computing, Cambridge Univ. Press, London/New York.
38. Qian, H., and Elson, E. L. (1990) *Biophys. J.* **57,** 375–380.
39. Anderson, S. R., and Weber, G. (1969) *Biochemistry* **8,** 371–377.
40. Rawitch, A. B., Hudson, E., and Weber, G. (1969) *J. Biol. Chem.* **244,** 6543–6547.
41. Thompson, N. L. (1991) *in* Topics in Fluorescence Spectroscopy (Lakowicz, J. R., Ed.), Vol. 1, pp. 337–378, Plenum, New York.
42. Rauer, B., Neumann, E., Widengren, J., and Rigler, R. (1996) *Biophys. Chem.* **58,** 3–12.
43. Berland, K. M., So, P. T. C., Chen, Y., Mantulin, W. W., and Gratton, E. (1996) *Biophys. J.* **71,** 410–420.
44. Chen, Y. (1999) *in* Biophysics, and Computational Biology, Univ. of Illinois at Urbana–Champaign, Urbana.
45. Göppert-Mayer, M. (1931) *Ann. Phys.* **9,** 273–295.
46. Friedrich, D. M. (1982) *J. Chem. Educ.* **59,** 472–481.
47. Denk, W., Strickler, J. H., and Webb, W. W. (1990) *Science* **248,** 73–76.
48. Berland, K. M. (1995) *in* Physics, Univ. of Illinois at Urbana–Champaign, Urbana.
49. Fischer, A., Cremer, C., and Stelzer, E. H. K. (1995) *Appl. Opt.* **34,** 1989–2003.
50. Xu, C., Guild, J., Webb, W. W., and Denk, W. (1995) *Opt. Lett.* **20,** 2372–2374.
51. Xu, C., and Webb, W. W. (1996) *J. Opt. Soc. Am. B Opt. Phys.* **13,** 481–491.
52. Mandel, L. (1979) *Opt. Lett.* **4,** 205–207.
53. Müller, J. D., Chen, Y., Ruan, Q. Q., Mantulin, W. W., and Gratton, E. (1999) *Biophys. J.* **76,** A359.
54. Fahey, P. F., Barak, L. S., Elson, E. L., Koppel, D. E., Wolf, D. E., and Webb, W. W. (1977) *Science* **195,** 305–306.
55. Palmer, A. G. d., and Thompson, N. L. (1989) *Proc. Natl. Acad. Sci. USA* **86,** 6148–6152.
56. Icenogle, R. D., and Elson, E. L. (1983) *Biopolymers* **22,** 1949–1966.
57. Weissman, M., Schindler, H., and Feher, G. (1976) *Proc. Natl. Acad. Sci. USA* **73,** 2776–2780.
58. Meyer, T., and Schindler, H. (1988) *Biophys. J.* **54,** 983–993.
59. Aragon, S. R., and Pecora, R. (1976) *J. Chem. Phys.* **64,** 1791–1803.
60. Mets, U., Widengren, J., and Rigler, R. (1997) *Chem. Phys.* **218,** 191–198.
61. Widengren, J., Dapprich, J., and Rigler, R. (1997) *Chem. Phys.* **216,** 417–426.
62. Sjoback, R., Nygren, J., and Kubista, M. (1995) *Spectrochim. Acta Part A* **51,** L7–L21.
63. Wang, J. H., and Graves, D. J. (1963) *J. Biol. Chem.* **238,** 2386–2389.
64. Wang, J. H., and Graves, D. J. (1964) *J. Biochem.* **3,** 1437–1445.
65. Ruan, K., and Weber, G. (1993) *Biochemistry* **32,** 6295–6301.
66. Huang, Y. C., and Graves, D. J. (1970) *Biochemistry* **9,** 660–671.